Self-Assembling Monomeric Nucleoside Molecular Nanoparticles Loaded with 5-FU Enhancing Therapeutic Efficacy against Oral Cancer

Hang Zhao,[†,‡,#] Hui Feng,[†,§,#] Dongjuan Liu,[†,#] Jiang Liu,[†,‡] Ning Ji,[†] Fangman Chen,[†] Xiaobo Luo,[†] Yu Zhou,[†] Hongxia Dan,[†] Xin Zeng,[†] Jing Li,[†] Congkui Sun,[†] Jinyu Meng,[†] Xiaojie Ju,[⊥] Min Zhou,[†] Hanshuo Yang,[∥] Longjiang Li,[†] Xinhua Liang,[†] Liangyin Chu,[⊥] Lu Jiang,[*,†] Yang He,[*,‡] and Qianming Chen[*,†]

[†]State Key Laboratory of Oral Diseases, West China Hospital of Stomatology, Sichuan University, Chengdu, Sichuan 610041, P. R. China, [‡]Institute for Nanobiomedical Technology and Membrane Biology, Regenerative Medicine Research Center, West China Hospital, West China Medical School, Sichuan University, Chengdu, Sichuan 610041, P. R. China, [§]XiangYa Stomatological Hospital, Central South University, Changsha, Hunan 410000, P. R. China, [⊥]School of Chemical Engineering, Sichuan University, Chengdu, Sichuan 610041, P. R. China, and [∥]State Key Laboratory of Biotherapy and Cancer Center, West China Hospital, and Collaborative Innovation Center for Biotherapy, Sichuan University, Chengdu, Sichuan 610041, P. R. China. [#]These authors contributed equally to this work.

ABSTRACT Conventional oligonucleotide based drug delivery systems suffer from lengthy synthetic protocols, high cost, and poor chemical or enzymatic stability under certain circumstances. Canonical free individual nucleosides cannot form stable nanostructures in aqueous solution as drug vehicles. Here, we report the development of a monomeric self-assembled nucleoside nanoparticle (SNNP) into an efficient drug delivery system which has currently no parallel in such field. This was achieved using a L-configurational pyrimido[4,5-*d*]-pyrimidine nucleoside building block that can form robust discrete nanoparticles in just one step with water as the sole solvent. Its high biocompatibility and low toxicity was demonstrated *in vitro* and *in vivo*. In mouse xenograft model of oral squamous cell carcinoma (OSCC), SNNP loaded with 5-fluoro-uracile (5-FU-SNNP) remarkably retarded the tumor growth compared with free 5-FU, albeit SNNP alone showed no antitumor effect. The stability in blood circulation and the effective concentration of 5-FU in tumor tissue were increased upon the loading with SNNP. TUNEL and immunohistochemistry analyses further indicated that the superior *in vivo* antitumor efficacy of 5-FU-SNNP compared to free 5-FU was associated with an enhanced degree of inhibition of cell proliferation and stimulation of cell apoptosis. Furthermore, SNNP alleviated the toxic side effects of 5-FU. These findings suggested that when loaded with SNNP, 5-FU has better antitumor efficacy and lower side effects, indicating that SNNP can efficiently act as a readily accessible, robust, biocompatible and low-toxic nanobiomaterial which may find wide therapeutic applications clinically in the future.

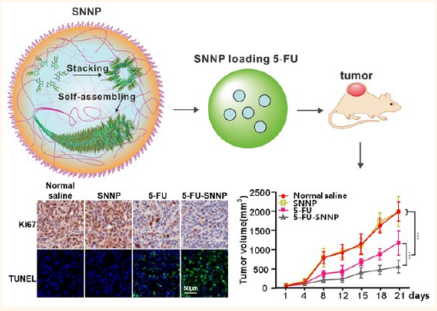

KEYWORDS: cancer therapy · drug delivery systems · J-TA ribonucleoside nanoparticles · self-assembled · 5-FU

Drug delivery systems are designed to improve bioavailability, reduce degradation, and alleviate the side effect of the loaded drugs. With the development of nanotechnology, drug delivery systems have received widespread attention, especially in the field of cancer therapy because of their ability to improve therapeutic efficacy.[1−5] Liposomes were first developed as drug carriers in the 1960s, other varieties of nanomaterials, including polymers, micelles and gels *etc.*, had been employed and shown promise as drug transport platform in this field over the past few decades.[6−11] Despite certain improved therapeutic advantages, some limitations still exist. For instance, some drug delivery systems may be toxic to normal tissues and sometimes may even result in a reduction of drug efficacy, because of the sophisticated procedures and excessive chemical treatments utilized in the preparation of some of these drug carriers. These limitations hinder the transformation of some drug carriers into clinical applications.[12−15] Therefore, an efficient delivery system with a relatively simple preparation procedure and low-toxicity is still a major challenge for the development of nanodrug-carriers. In nature, biological macromolecules (nucleic acids,

* Address correspondence to jianglu@scu.edu.cn, heyangqx@scu.edu.cn, qmchen@scu.edu.cn.

Received for review January 17, 2015 and accepted September 8, 2015.

Published online September 08, 2015
10.1021/acsnano.5b04520

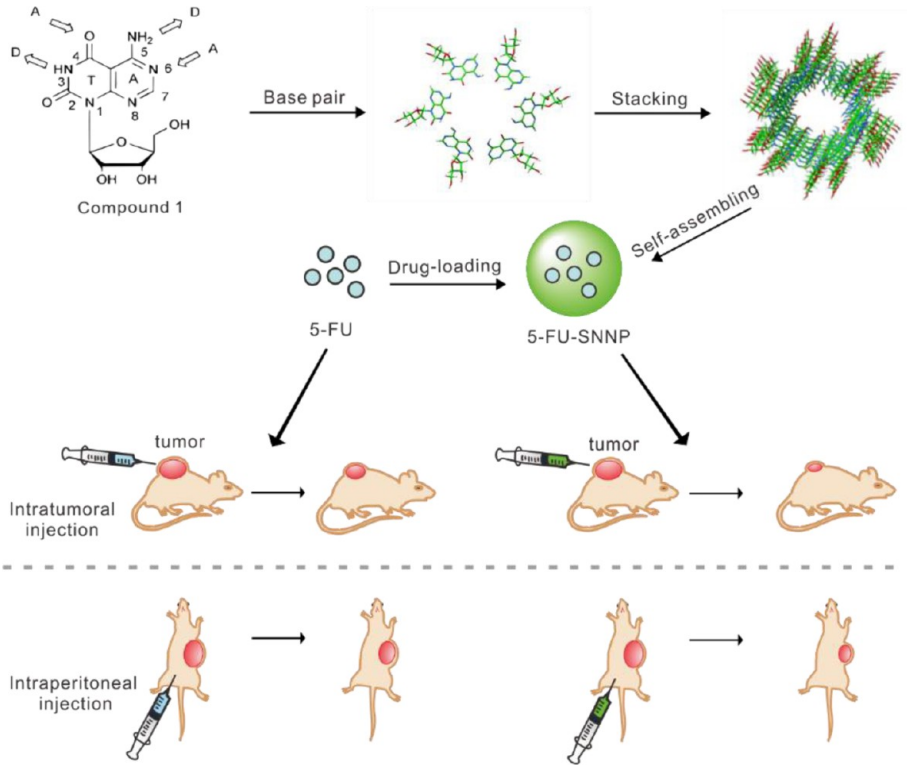

Figure 1. Dynamic representation of SNNP preparation and comparison of anticancer efficacy of 5-FU and 5-FU-SNNP using intratumoral and intraperitoneal injection administration methods.

protein and olig/poly saccharides) are not only serving many sophisticated biological functions, but are also endowed with special uses in the field of nanotechnology for their well-defined spatial arrangements constructed *via* hierarchical assembly from building blocks to higher-order structures. Among these biological macromolecules, nucleic acid analogues have been used as drug delivery system because of their unique complementarity, biocompatibility, and thermal stability.[16,17] However, due to their poor chemical and enzymatic stability *in vivo*, together with the high cost of mass production resulting from the lengthy and sophisticated solid-phase synthesizing methodologies, their wide applications as drug carriers in large scale are hampered under certain circumstances. Although there were also some self-assemblied nucleolipids used as carriers[18,19] and lipidic nucleoside prodrugs formulated as nanoassemblies to enhance the drug's efficacy,[20,21] the rich chemistry and highly diverse structures of monomeric nucleoside analogues are not yet fully exploited in this field.

To tackle these problems, we are committed to studying the possibilities of using only base moiety modified monomeric nucleoside molecules as drug delivery system. Initially, we synthesized a tridentate Janus-type guanosine−cytosine (J-GC) nucleoside and found that it indeed formed nanobundles with Watson−Crick base pairing in a dimethylformamide (DMF) solution. However, the associated cytotoxicity prevents its utility for this purpose.[22] Later, we synthesized a bidentate Janus-type thymidine−adenosine (J-AT) nucleoside and found that it can form flower-shaped superstructures in aqueous solvent with uniform diameters of around 40 μm.[23,24] Unlike J-GC nucleoside, the cytotoxicity of J-AT nucleoside was quite low. However, it was also not suitable as drug delivery system due to its micrometer-ranged size. Since the whole shape and size of this type of supramolecular assembly strongly depend on the chemical structure of individual building blocks, especially the configuration and conformation around the glycosidic bond, we therefore designed and synthesized the L-configurationed J-TA ribonucleoside (**1**) by transglycosylation reaction. Interestingly, the monomeric J-TA L-ribonucleoside (**1**) can self-assemble in water to form uniformly sized distribution of discrete nanoparticles (~150 nm). The base moiety of compound **1** had both the Watson−Crick H-bond acceptor−donor (AD) pattern of thymidine and the donor−acceptor (DA) pattern of adenine (Figure 1). According to our previously reported theoretical calculations,[23] the mechanism of nanoparticle formation by compound **1** may be as follows: first, a six-membered supermacrocycle is constructed *via* H-bondings through Watson−Crick base pairs; second, these six-membered rings stacked layer by layer to form rosette nanotubes; and finally, the nanotubes further associate into higher ordered nanoparticles. Thus, the current supramolecular assembly consists of monomeric nucleoside molecules without the nuclease labile phosphodiester backbones. The additional

functional groups on the pyrimido[4,5-*d*]pyrimidine heterocyclic rings offer more self-complementary hydrogen bond acceptor and donor positions, which will form more stable hydrogen bond networks compared to canonical nucleosides, which in turn makes the monomeric building blocks into robust discrete nanoparticles even in the competitive aqueous surroundings. Additionally, the base stacking might also be stronger than canonical pyrimidine and purine nucleosides due to the increasing surface area of base moiety. Besides these modified base moiety, the unusual L-configuration of the sugar residue may offer its additional resistance against other nucleoside metabolic enzymes. So the overall stability of our current new system should be superior to the oligonucleotide-based delivery system. Furthermore, from the preparation point of view, this novel self-assembled nucleoside nanoparticle (SNNP) has the added benefits of a simpler preparation procedure, a greener process (only water as solvent) and of being biodegradable compared with other traditional drug carriers.

Oral squamous cell carcinoma (OSCC) is the sixth most common malignancy worldwide.[25−29] Despite the increasing development of chemotherapy, the prognosis of patients with this kind of malignancy is still rather poor.[30,31] One of the most important reasons is the low therapeutic efficiency of the anticancer drugs. 5-Fluoro-uracil (5-FU) is a pyrimidine analogue that interferes with thymidylate synthesis. It was first described in 1957 and has remained an essential component of chemotherapy for a number of solid tumors, particularly head and neck malignancies including OSCC.[32] Unfortunately, limitations such as its short biological half-life resulting from rapid metabolism, toxic side effects on bone marrow, and nonselective action against healthy cells limited the role of 5-FU in systemic therapy of these tumors.[33−37] To overcome the drawbacks of 5-FU, various nanoparticles were developed for the delivery of 5-FU to the cancer tissues, which can enhance the antitumor efficacy of 5-FU to a certain extent *in vivo*.[38,39] Inspired by these, we would like to investigate if 5-FU can be encapsulated in the aforementioned SNNP and whether its antitumor efficacy can be improved accordingly. The rationale behind this thought is that 5-FU is a thymine derivative which might be entrapped by SNNP through base−base interactions between them, and thus, SNNP may function as a drug carrier for the delivery of 5-FU in the body.

In this study, we present the preparation and characterization of a SNNP drug delivery system loaded with 5-FU. The objectives of this study were to evaluate the potential of using the SNNP as drug delivery system to alleviate the limitations of 5-FU such as short biological half-life and toxic side effects. Specifically, we compared the ability to inhibit tumor growth of 5-FU-SNNP to free 5-FU in a mouse xenograft model of OSCC. In general, we demonstrated that SNNP has high biocompatibility and low cytotoxicity both *in vitro* and *in vivo*. The stability in blood circulation and the effective concentration of 5-FU in tumor tissue was increased upon the loading with SNNP. Most importantly, 5-FU-SNNP markedly retarded the *in vivo* growth of OSCC xenografts in mouse models compared with free 5-FU. Meanwhile, SNNP also decreased the toxic side-effects of 5-FU. Because of all these advantages, plus the readily accessibility of the monomeric building blocks and greener process of nanoparticles, this new type of SNNP has a high hope to be a promising candidate nanoparticle-delivery strategy for cancer therapy clinically in the future.

RESULTS AND DISCUSSION

Synthesis and Characterization of SNNP. Nanoparticles can preferentially deliver chemotherapeutics to tumors due to their Enhancement Permeation and Retention (EPR) effect. Therefore, they have become key vehicles for the delivery of anticancer drugs.[40] Due to their unique complementarity and biocompatibility, nucleic acid analogues have been proven to be versatile building blocks for constructing differently shaped nanomaterials (such as nanoparticles) for drug delivery applications. However, their high cost and poor chemical and enzymatic stability *in vivo* may restrict its application in the field of drug delivery. To solve this problem, we set out to construct novel drug delivery carriers by monomeric nucleoside molecules. In this study, we designed and synthesized the J-TA L-ribonucleoside and found that it can form discrete nanoparticles by self-assembling in water. For the synthesis of J-TA L-ribonucleoside (**1**), the transglycosylation reaction was adopted.[23] The compound of J-AT L-acetylated was treated with HMDS and xylene to afford the silylated intermediate. Then, the intermediate compound was rearranged to afford compound **2**. Subsequently, the target compound **1** was successfully obtained as a white powder by removing the acetyl groups from **2**. The structures of compounds **1** and **2** were thoroughly characterized using NMR, HRMS, and UV, in addition, the CD spectra of the D- and L-enantiomers of J-TA nucleosides displayed a exact mirror image (Figure S1). To prepare the SNNP, compound **1** was dissolved in water, heated to 100 °C, and cooled at room temperature for 24 h. SEM and DLS showed that compound **1** formed SNNP with uniform diameters around 150 nm (Figure 2A). Compared with RNA/DNA NPs, these SNNP have a simpler preparation procedure (single step) and greener process (water as the sole solvent). Next, the finer structure of the SNNP was revealed by TEM, which gave us visual evidence that these SNNP consisted of many nanotubes (Figure S2). To further study the hydrogen bonds formation of the SNNP spectroscopically, the VT NMR experiment was carried out, which indicated that the formation of this SNNP was indeed engaging certain intermolecular

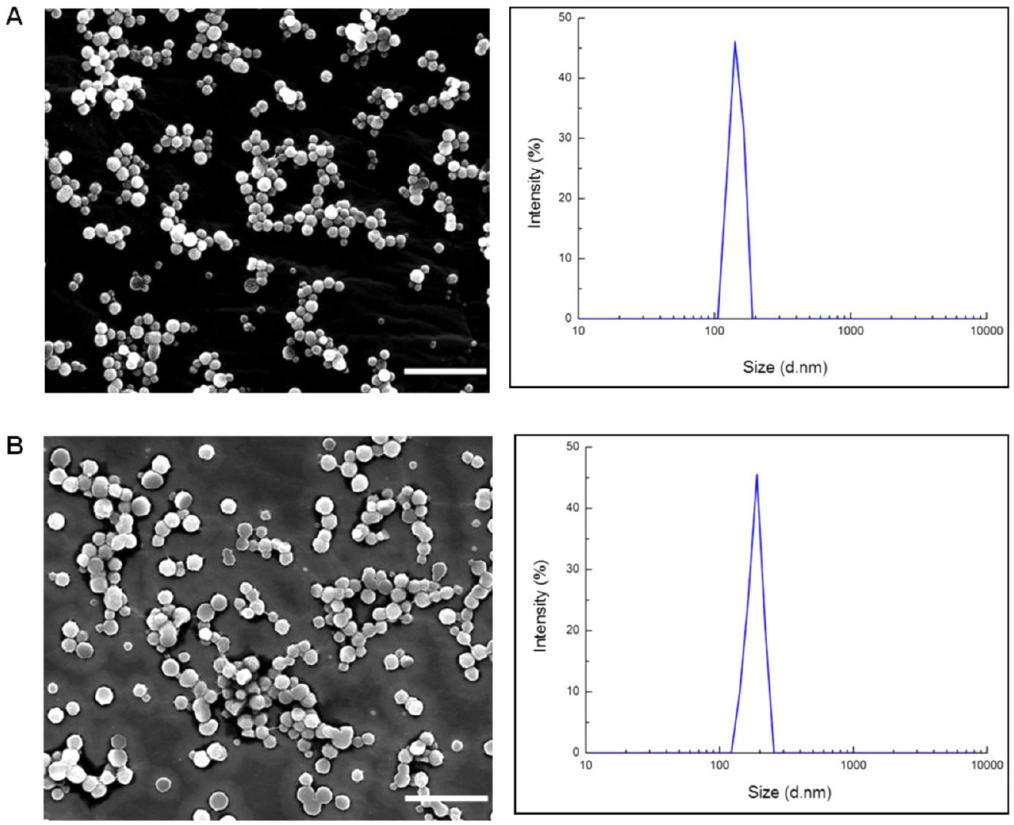

Figure 2. Diameter (volume) distribution of SNNP and 5-FU-SNNP analyzed by SEM and DLS. (A) SEM images and DLS regularization of compound 1 (0.1 mg·mL^{-1} in water, the average hydrodynamic radius recorded is 150 nm (average of 10 measurements, Nano-ZS, Malvern). (B) SEM images and DLS regularization diagrams of 5-FU-SNNP (the average hydrodynamic radius recorded is 200 nm (average of 10 measurements, Nano-ZS, Malvern). Scale bars: 2 μm.

hydrogen bonds between individual nucleosides (Figure S3). The critical melting temperature (T_m) for the disassembly of this SNNP was measured by Variable Temperature Fluorescence (VT FL) spectroscopy technique to be 67.5 °C (Figure S4). Meanwhile, the storage stability results indicated that the SNNP were stable for up to 60 days at room temperature, and it was stable over a wide pH range from 4 to 11. Moreover, the SNNP was stable enough in preheated 90% fetal bovine serum (FBS) (1:9 v/v) at 37 °C within 12 h (the overall assembly is kept intact); the morphology and size of the nanoparticles only began to change slightly up to 24 h incubation (Figure S5). These data proved that this SNNP should be also stable enough under the physiological conditions. Considering the J-AT ribonucleoside is a mimic of natural nucleosides, they might have a good biocompatibility.

Drug Loading and Releasing Behavior *in Vitro*. To utilize this type of SNNP as drug delivery vehicles, the drug-loading experiments were carried out: the J-TA L-ribonucleoside (compound **1**) was dissolved in PBS; the solution was heated to ~100 °C and allowed to cool to room temperature for ~24 h. Then, the 5-FU was added into the solution and this wasaged for 24 h to allow the drug-loading process to complete. To confirm the success of drug loading, SEM and DLS analyses were performed. SEM indicated almost no morphological change between the original SNNP and the drug loaded SNNP. DLS experiments further showed the size distribution of 5-FU-SNNP to be 200 nm approximately, which was obviously bigger than SNNP-without-loading (Figure 2B). The loading capability and encapsulation efficiency of the 5-FU loaded SNNP were identified to be about 35% and 53%, respectively (Table S1). The NMR experiments showed that the hydrogen atoms N11H and 5-FU–C6-H were involved in the formation of intermolecular hydrogen-bond in the process of 5-FU loaded with SNNP (Figures S6 and S7). To further study whether the hydrogen bonding from 5-FU will disturb the thermo stability of the whole assembly, the Variable Temperature Fluorescence (VT FL) of the 5-FU-SNNP was carried out and the T_m value of this assembly was measured to be 61.5 °C, 6 °C lower than that of free SNNP (Figure S8). This phenomenon indicates that the additional competitive hydrogen bonds due to the presence of 5-FU loaded into SNNP indeed slightly destabilize the whole assembly, but the relative high melting temperature of the 5-FU-SNNP indicates it should be stable enough under physiological temperature. Once the loading capacity of SNNP was validated, the next step was to investigate its release behavior *in vitro*. From the results shown in Figures S9 and S10, the total release profile of 5-FU-SNNP (~47% of 5-FU release from the particle)

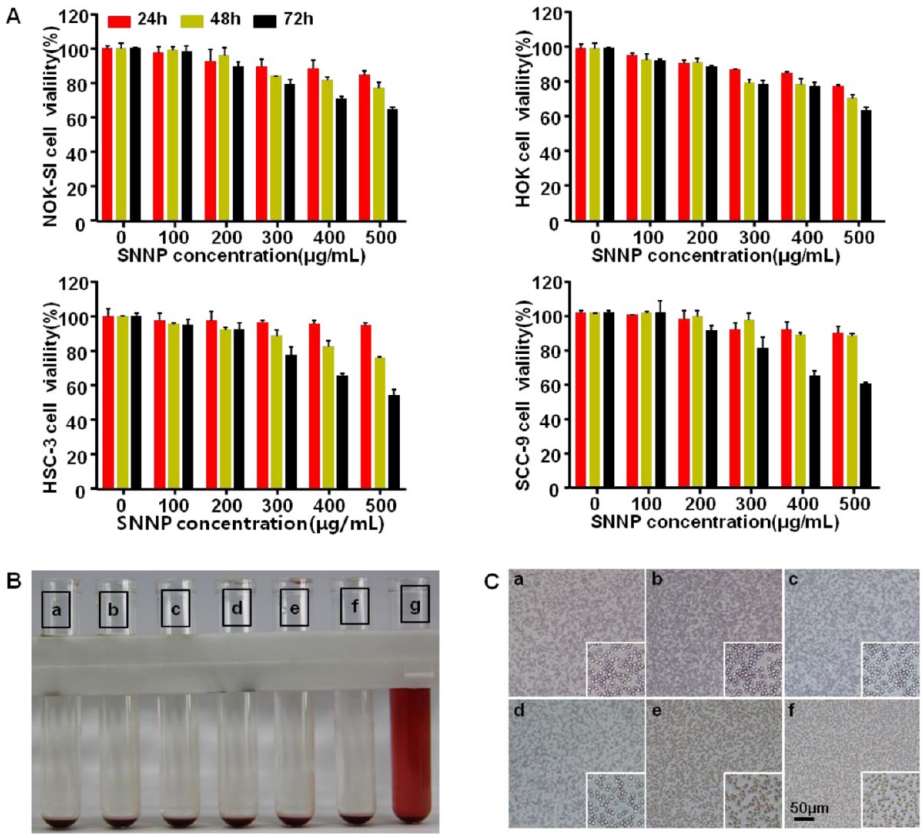

Figure 3. SNNP had low acute toxicity *in vitro*. (A) MTT assay of the cytotoxicity of free SNNP on immortalized normal oral keratinocyte cells (NOK-SI, HOK16E6E7) and OSCC cells (HSC-3, SCC-9). (B) Hemolytic assay. (C) Hemagglutination assay. The concentrations of SNNP were 500 $\mu g \cdot mL^{-1}$ (a); 400 $\mu g \cdot mL^{-1}$ (b); 300 $\mu g \cdot mL^{-1}$ (c); 200 $\mu g \cdot mL^{-1}$ (d) and 100 $\mu g \cdot mL^{-1}$ (e), respectively. Normal Saline (f) used as negative control. Distilled water (g) used as positive control. Data represent 3 independent experiments. Data presented as mean ± SD (n = 4). Scale bar: 50 μm.

exhibited two stages: first, a relatively faster release period (burst release), in which ~24% of 5-FU was already released from the SNNP within the initial 11 h; second, a relatively slower release period (sustained release), in which the remaining ~23% of 5-FU was released from SNNP within the next 325 h. Therefore, these results suggested that SNNP can be used as a potential drug delivery system.

Evaluation of Acute Toxicity of SNNP *in Vitro*. Since the potential toxicity of biomaterial itself may hinder its application as drug carrier,[41−43] nontoxic or low-toxic biomaterials are hotspots for the research of drug delivery systems.[44−46] To evaluate the biosafety of SNNP to be used as drug carrier, we studied the toxicity of SNNP both *in vitro* and *in vivo*. The *in vitro* acute toxicity of SNNP was evaluated by MTT assay and blood compatibility assay. The MTT assay was conducted in both immortalized normal oral keratinocyte cells (NOK-SI, HOK16E6E7) and OSCC cells (HSC-3, SCC-9). The results showed that the cytotoxicity of SNNP displayed a concentration and time-dependent manner. As shown in Figure 3A, there is a negative correlation between the cell viability and SNNP concentration and the incubation time. The cell viability decreased from 100% to ~60% with the increase of SNNP concentration from 100 to 500 $\mu g \cdot mL^{-1}$ and the incubation time from 24 to 72 h. It is worthwhile mentioning that the viability of cells incubated with 100 $\mu g \cdot mL^{-1}$ SNNP did not change obviously during the observed 72 h. Moreover, no significant differences were observed between normal cells and OSCC cells. We further tested the blood compatibility of SNNP by hemolysis and hemeagglutination assays.[47−50] As shown in Figure 3B, SNNP at all concentrations (from 100 to 500 $\mu g \cdot mL^{-1}$) were nonhemolytic compared with distilled water used as positive control. Moreover, as shown in Figure 3C, no agglutination was detected when erythrocytes were in touch with naked SNNP of all tested concentrations compared with saline used as negative control. Thus, our *in vitro* studies indicated SNNP to be a blood-compatible biomaterial used for drug delivery platform with nontoxic or low-toxic to cells particularly at a concentration of 100 $\mu g \cdot mL^{-1}$.

Evaluation of Acute Toxicity of SNNP *in Vivo*. To further evaluate the biosafety of SNNP *in vivo*, SNNP was injected intraperitoneally to mice at different concentrations (0.5, 2.5, and 5 $mg \cdot kg^{-1}$) once a week for 2 weeks using normal saline as negative control. Complete blood count (CBC), serum biochemical indicators and histological examination were performed

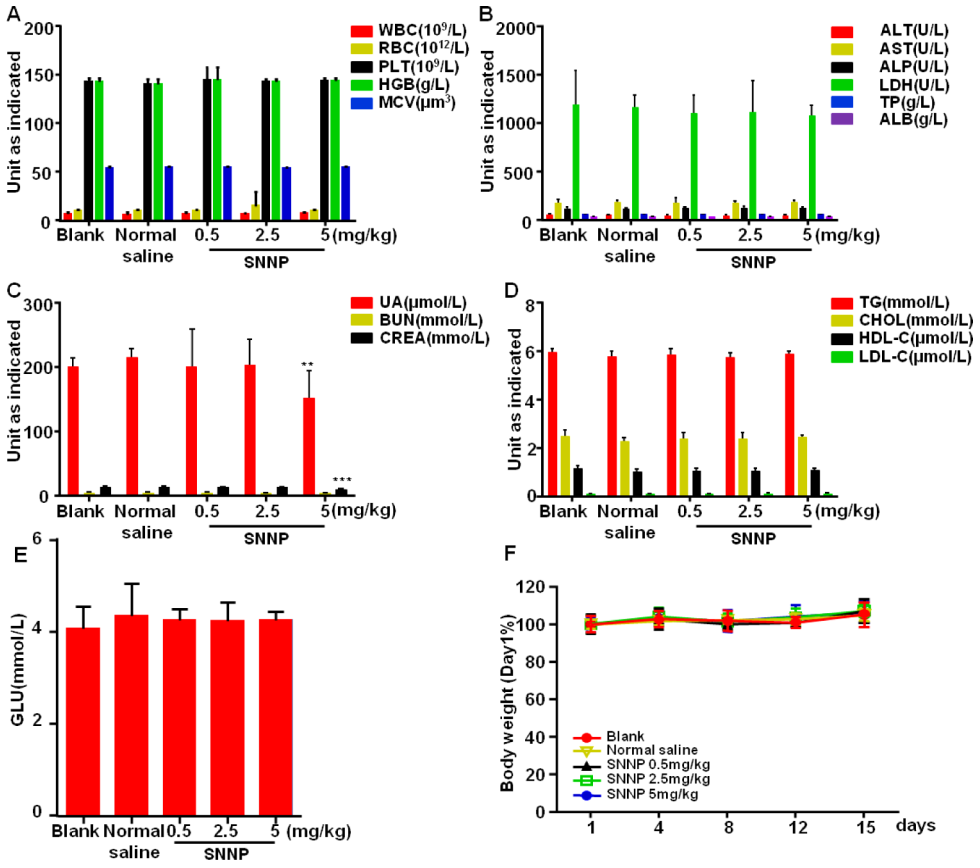

Figure 4. SNNP had low acute toxicity *in vivo*. SNNP were injected to mice intraperitoneally at the concentration of 0.5, 2.5, and 5 mg·kg^{-1}, respectively, once a week using normal saline as negative control for 2 weeks. (A) Hematological analysis. (B−E) Serum biochemistry analysis. (F) The body weight curves of all groups. The results represent mean ± SD (n = 8, *P < 0.05, **P < 0.01, ***P < 0.001).

to evaluate the acute toxicity of SNNP.[51−53] CBC did not suggest any acute toxicity of SNNP at all tested concentrations (Figure 4A). The results of serum biochemical indicators showed decrease of plasma UA (**P < 0.01) and CREA (***P < 0.001) in 5 mg·kg^{-1} SNNP treated mice, while no significant differences were found in biochemical indices between free SNNP treatment groups (0.5, 2.5 mg·kg^{-1}) and the control groups (P > 0.05) (Figure 4B−E).

On the basis of the results of histological examination by Hematoxylin and Eosin (H&E) staining assay, no noticeable signs of organ damage were found in the heart, liver, spleen, lung or kidneys of treatment groups compared with control groups (Figure 5). During the whole experiment, neither animal death nor behavioral abnormalities were observed in the control or treated groups. Moreover, body weights of the treated animals were statistically identical to the control groups (Figure 4F). According to these results, SNNP showed low toxicity both *in vitro* and *in vivo*. Its safety concentration was 100 μg·mL^{-1} *in vitro* and below 5 mg·kg^{-1} *in vivo*. So it has the latent capacity to be used as drug delivery platform.

SNNP Increased the Stability of 5-FU in Blood Circulation. To see whether SNNP can increase the stability of 5-FU in blood circulation, we studied the pharmacokinetics of 5-FU-SNNP by measuring the concentration of 5-FU in the blood over time (Figure 6) after intravenous injection of 5-FU-SNNP into OSCC xenografted BALB/c nude mice using equal amount of 5-FU as control. Blood of mice was drawn from the posterior venous plexus of the eye at each time point post injection (p.i.) and measured by LC−MS/MS. The blood circulation curve showed that compared with free 5-FU, 5-FU-SNNP got a much higher blood concentration of 5-FU at the same time point p.i., moreover, the $t_{1/2z}$ of 5-FU in 5-FU-SNNP group was 6.43 ± 5.94 h compared with 3.64 ± 2.2 h in the free 5-FU group, and $AUC_{0-\infty}$ was 4919.46 ± 536.50 and 2401.21 ± 263.21 μg·L^{-1}·h^{-1} in these two groups, respectively. These results indicated that SNNP can increase the stability of 5-FU in blood circulation and therefore effectively prolong the circulation time of 5-FU.

SNNP Led to Increase Uptake of 5-FU in OSCC Xenograft Tumor Tissue. To study the difference between the biodistribution of 5-FU in 5-FU-SNNP and free 5-FU groups, xenografted BALB/c nude mice were sacrificed at 5, 15, 45, 90, and 240 min p.i. of 5-FU-SNNP and 5-FU, respectively. Various organs and OSCC xenograft tumor tissues were collected and measured by the

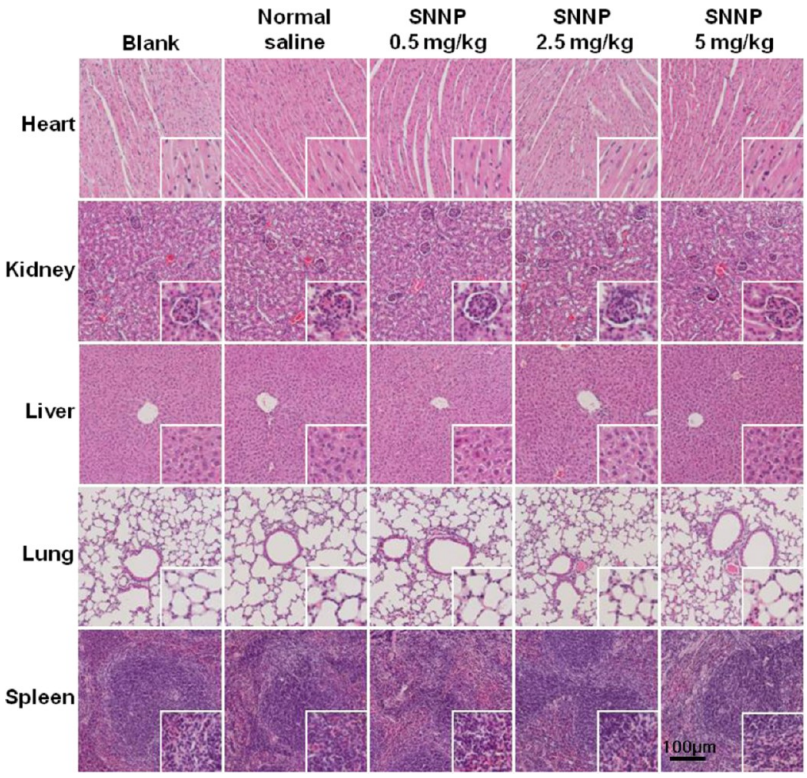

Figure 5. Hematoxylin and eosin (H&E) staining assay of heart, kidney, liver, lung, and spleen tissues after intraperitoneal injection of different concentrations of free SNNP (0.5, 2.5, and 5 mg·kg^{-1}, respectively) once a week for 2 weeks. Experiments repeated 3 times. Scale bar: 100 μm.

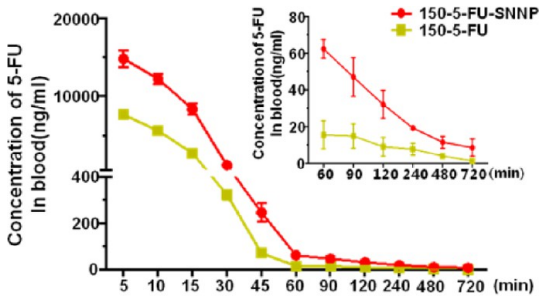

Parameter(mean±SD)	5-FU	5-FU-SNNP
AUC_{0-t}(ug/L*h)	2357.73 ± 302.71	4863.46 ± 551.89
$AUC_{0-\infty}$(ug/L*h)	2401.21 ± 263.22	4919.461 ± 536.51
$t_{1/2z}$(h)	3.64 ± 2.2	6.43 ± 5.94
T_{max}(h)	0.052 ± 0.05	0.038 ± 0.02
CL_z(L/h/kg)	63.16 ± 7.65	30.826 ± 3.71
C_{max}(ug/L)	10006.7 ± 1438.84	18481.5 ± 4360.07

Figure 6. Blood circulation curve of 5-FU-SNNP and free 5-FU. Error bars were based on standard deviations of 6 mice per time point. Inset table: pharmacokinetic data of 5-FU-SNNP and free 5-FU (including AUC_{0-t}, $AUC_{0-\infty}$, $t_{1/2z}$, T_{max}, CL_z, and C_{max}).

LC−MS/MS. We found that upon injection of free 5-FU, 5-FU distributed in many different organs and OSCC xenograft tumor tissues, with the highest accumulation in the kidneys followed by heart, OSCC xenograft tumor tissue, lung and liver (Figure 7). Upon injection of 5-FU-SNNP, the uptakes of 5-FU increased significantly in all the tested organs and OSCC xenograft tumor tissues (Figure 7). It is worth noting that the 5-FU levels in all the tested organs and OSCC xenograft tumor tissues decreased very fast after 45 min p.i.; however, it decreased much slower in OSCC xenograft tumor tissues compared with other organs upon loading by SNNP. At 45, 90, and 240 min p.i., the OSCC xenograft tumor tissue uptake was 9.00, 5.81, and 5.06% ID/g, respectively. These results suggested that due to the sustained-release effect of SNNP and the subsequent increased passive tumor targeting effect, SNNP leads to increased uptake of 5-FU in OSCC xenograft tumor tissues.

SNNP Enhanced Anticancer Efficacy of 5-FU by Using Intratumoral and Intraperitoneal Injections on OSCC Xenograft Mouse Model. Drug delivery system is designed to improve the therapeutic efficacy and decrease side effects of the loaded drugs.[42,48,49,53−57] To investigate the antitumor efficacy of 5-FU-SNNP compared to free 5-FU, first we used intratumoral injection as a localized treatment on OSCC xenograft mouse model. Three different concentrations of 5-FU (75,150, and 300 mg·kg^{-1}) were used to treat HSC-3 cell OSCC xenografts. For each concentration, tumor-bearing mice were randomly divided into 4 groups (n = 6): control group treated with normal saline, SNNP group treated with 5 mg·kg^{-1} SNNP, 5-FU group treated with certain concentration of 5-FU, and 5-FU-SNNP group treated with 5 mg·kg^{-1} SNNP loading equal amount of 5-FU used in 5-FU group. Mice were treated once per week

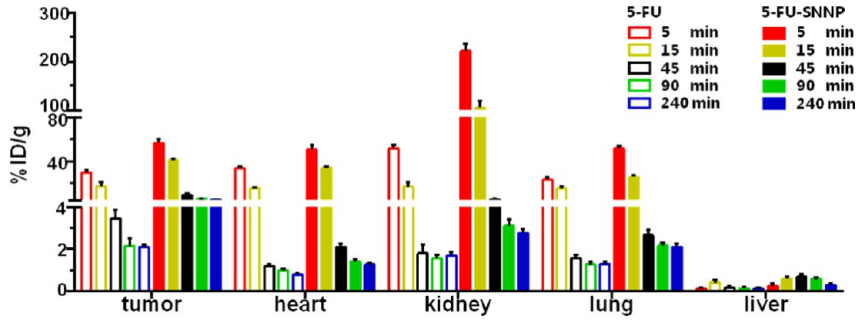

Figure 7. Time-dependent biodistribution of 5-FU in different organs and OSCC xenograft tumor tissues upon iv injection of free-5-FU and 5-FU-SNNP.

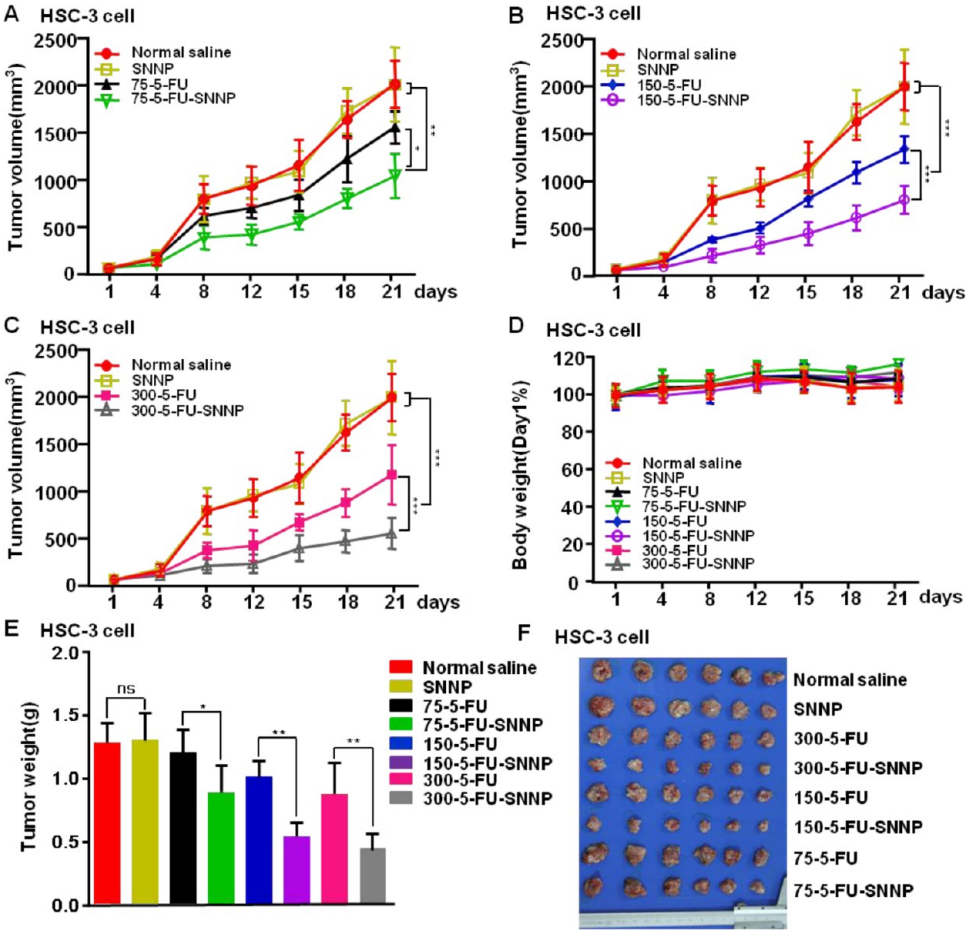

Figure 8. 5-FU-SNNP had a greater anticancer efficacy compared with 5-FU on OSCC xenograft mouse model through intratumoral injection. Tumor growth curves (A–C) and mice body weight curves (D) of 5-FU/5-FU-SNNP (75, 150, and 300 mg·kg^{-1}, respectively) treated groups using normal saline and free SNNP as controls. Average tumor weight (E) and images of xenografts (F) at the end of experiment. The results represent mean ± SD (n = 6, *P < 0.05, **P < 0.01, ***P < 0.001).

through intratumoral injection for 2 weeks (injections on day 1, 7 and 14) and monitored for an additional 1 week to observe tumor growth. The volume of the tumors during treatment is shown in Figure 8A–C, and the final tumor weight at the end of 3 weeks is depicted in Figure 8E. At the end of three week of treatment, tumors from mice in the saline and free SNNP treated group had grown significantly, those from the free 5-FU treated group showed a much slower growth, and those treated with 5-FU-SNNP showed the smallest increase in tumor volume. This difference increased with the increase of 5-FU concentration. At the end of 3 weeks, with 75 mg·kg^{-1} 5-FU, the average tumor volumes of free 5-FU and 5-FU-SNNP treated groups were about 70% and 60%, respectively, of these control groups. When the concentration of 5-FU increased to 150 and 300 mg·kg^{-1}, the average tumor volumes of free 5-FU and 5-FU-SNNP groups decreased to about 70% and 45%, and 60% and 25%, respectively, of the control groups. Therefore, the 5-FU-SNNP displayed a

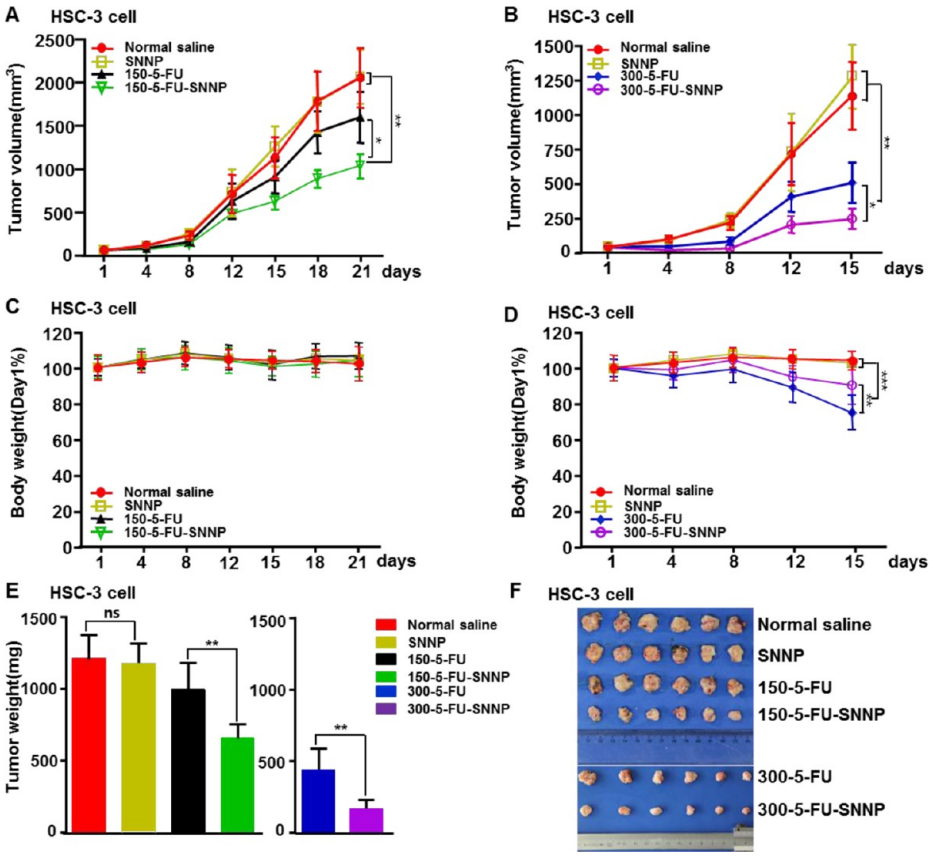

Figure 9. 5-FU-SNNP had a greater anticancer efficacy compared with 5-FU on OSCC xenograft mouse model through intraperitoneal (ip) injection. Tumor growth curves (A and B) and mice body weight curves (C and D) of 5-FU/5-FU-SNNP (150 and 300 mg·kg^{-1}, respectively) treated groups using normal saline and free SNNP as controls. Average tumor weight (E) and images of xenografts (F) at the end of experiment. The results represent mean ± SD (n = 6, *P < 0.05, **P < 0.01, ***P < 0.001).

much more significant degree of tumor growth inhibition compared with free 5-FU. It should be noted that there was no obvious difference between the tumor growth of the saline and free SNNP treated groups. Therefore, SNNP itself alone has no therapeutic effect on OSCC xenografts. As mentioned above, 5-FU has a rapid metabolism which limited its role in therapy of tumors. On the basis of these results, we deduced that the enhanced anticancer efficacy of 5-FU-SNNP was caused by the delayed release of 5-FU by SNNP which allowed 5-FU to produce a long-term effect compared to free 5-FU. Therefore, SNNP can serve as a drug delivery vehicle which can enhance the efficacy of the loaded agent. During the whole experiment, no significant differences were found among the average body weight of these groups.

To prove the effectiveness of the 5-FU-SNNP as a systemic treatment, we changed the administration method to intraperitoneal injection using two different concentrations of 5-FU (150 and 300 mg·kg^{-1}) and conducted it weekly for 3 weeks using the same OSCC xenograft mouse model. For each concentration, tumor-bearing mice were randomly divided into 4 groups with 6 mice each. As shown in Figure 9A,B, during the treatment, tumors from the free 5-FU treated group and 5-FU-SNNP treated group showed a significant inhibition of tumor growth compared with tumors from mice in the saline and free SNNP treated groups. 5-FU-SNNP also showed an enhanced anticancer efficacy compared with free 5-FU. At the end of the experiment, the average tumor weight of 150 and 300 mg·kg^{-1} 5-FU-SNNP treated groups reached about 70% and 45% of that of 150 and 300 mg·kg^{-1} free 5-FU treated groups, respectively (Figure 9E). Therefore, the intraperitoneal injection experiment confirmed that SNNP can also serve as a drug delivery system to enhance the anticancer efficacy under systemic treatment. It is worth mentioning that, during the experiment, no significant differences were found among the average body weight of these groups when the concentration of 5-FU was 150 mg·kg^{-1} (Figure 9C). However, when 5-FU reached 300 mg·kg^{-1}, significant decrease of body weight was found in 5-FU and 5-FU-SNNP treated groups compared with the control groups. Moreover, the decrease was much more dramatic in the free 5-FU treated group (Figure 9D). On day 15, two of six mice died in the free 5-FU group, while no mouse died in the 5-FU-SNNP group. Therefore, it seemed that SNNP can reduce the toxic side effects of 5-FU on bone marrow and healthy cells to some extent. To sum up, the results of intraperitoneal injection confirmed that SNNP itself alone has no therapeutic effect

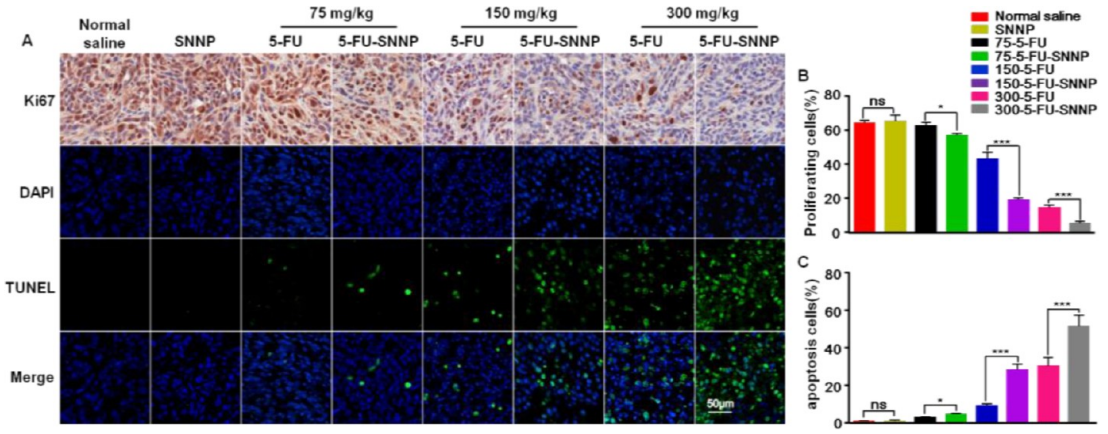

Figure 10. Effect of inhibiting cell proliferation and stimulating apoptosis by 5-FU in OSCC xenografts was enhanced in 5-FU-SNNP. (A) Immunohistochemistry analysis of Ki67 and TUNEL staining of apoptosis cells in OSCC xenograft tissues. Rate of cell proliferation (B) and cell apoptosis (C) in OSCC xenograft tissues of different groups. Results represent mean ± SD ($n = 6$, *$P < 0.05$, **$P < 0.01$, ***$P < 0.001$). Scale bar: 50 μm.

on OSCC xenografts, and SNNP can significantly enhance the anticancer efficacy of 5-FU on OSCC. Moreover, SNNP can even reduce the toxic side effects of 5-FU.

The Effect of Inhibiting Cell Proliferation and Stimulating Apoptosis by 5-FU in OSCC Xenografts Was Enhanced in 5-FU-SNNP. To further investigate the underlying mechanism of enhanced anticancer effect of 5-FU-SNNP compared with free 5-FU, cell proliferation and cell apoptosis in OSCC xenograft tumor tissue were studied. Ki67, a marker of cellular proliferation, was detected by immunohistochemistry assay. As shown in Figure 10A, Ki67 expression decreased significantly with the increase of 5-FU concentration. Moreover, 5-FU-SNNP treated tumors revealed much more significant decrease of the proportion of Ki67 positive cells compared to the free 5-FU treated ones. In the 75 mg·kg^{-1} 5-FU groups, the average percentage of Ki67 positive cells in 75 mg·kg^{-1} 5-FU and 5-FU-SNNP groups were 62.77% and 57.02%, respectively; in the 150 mg·kg^{-1} groups, they were 43.41% and 19.42%, respectively; in the 300 mg·kg^{-1} groups, they were 14.97% and 5.81%, respectively (Figure 10B). Cell apoptosis was further studied by TUNEL assay. The results showed that compared with free 5-FU treated OSCC xenografts, 5-FU-SNNP treated ones revealed much higher cell apoptosis rate, and this became more significant with the increase of 5-FU concentration (Figure 10A). As shown in Figure 10C, the average cell apoptosis rates of the 75, 150, and 300 mg·kg^{-1} free 5-FU treated tumors were 2.69%, 8.68%, and 29.84%, respectively; while those of the 75, 150, and 300 mg·kg^{-1} 5-FU-SNNP groups were 4.24%, 27.96%, and 51.20%, respectively. At the same time, the average cell apoptosis rates of saline and free SNNP treated groups were only 0.59% and 0.58%, respectively. Our results suggested that the effect of inhibiting cell proliferation and stimulating apoptosis by 5-FU in OSCC xenografts was enhanced in 5-FU-SNNP.

CONCLUSIONS

In summary, we designed and synthesized a Janus type L-configurational J-TA ribonucleoside (**1**) by transglycosylation reaction. It can form robust discrete SNNP by self-assembling in water, which is the first reported nanoparticle formed by monomeric nucleoside molecule in water. This type of SNNP was further demonstrated to have low toxicity both *in vitro* and *in vivo*. Through serum pharmacokinetics and biodistribution studies, SNNP was found to increase the stability of 5-FU in blood circulation, and thus, *via* the sustained-release effect of SNNP and the following increased passive tumor targeting effect, the accumulation of 5-FU in tumor area can be significantly improved. In a mouse xenograft model of OSCC, compared with free 5-FU, 5-FU-SNNP displayed a superior *in vivo* anticancer efficacy. Meanwhile, SNNP itself had no therapeutic effect on OSCC xenografts. Further studies showed an increased cell apoptosis and inhibited cell proliferation induced by 5-FU-SNNP compared with free 5-FU. In addition, SNNP alleviated the toxic side effects of 5-FU. Therefore, our studies distinguished the SNNP drug delivery platform as an efficient and relatively safe candidate to deliver nucleoside drug in the treatment of oral cancer.

MATERIALS AND METHODS

General. The J-TA L-ribonucleoside compound was synthesized in our laboratory. SEM was performed using a high resolution INSPECT F50. The UV absorption spectra were recorded on a DU-800 spectrophotometer, Beckman) (λ_{max} in nm, ε in dm^3 mol^{-1} cm^{-1}). Thin-layer chromatography (TLC) was performed on aluminum sheet covered with silica gel 60 F254 (0.2 mm, Merck, Germany). Flash column

chromatography (FC): silica gel 60 (Haiyang chemical company, P. R. China) at 0.4 bar. NMR spectra were recorded on a AV II (Bruker, Germany) spectrometer at 400 and 600 MHz; the δ values in ppm are relative to Me_4Si as internal standard. High resolution mass spectra were measured with mass analyzer (Q-TOF, Bruker, Germany). TEM images were recorded on a Tecnai G2 F20 microscope operated at 200 kV. 5-Fluoro-2,4 (1*H*,3*H*) pyrimidinedione (5-FU) was purchased from Sigma−Aldrich. The solvents and reagents were analytic pure. Solvents 1,2-dichloroethane and acetonitrile were purified by distilling from P_2O_5. All reagent water used in the laboratory was pretreated with the Milli-Q Plus System. All other reagents used were commercially available and analytical grade.

Cell Culture and Animals. Two OSCC cell lines (HSC-3, SCC-9) and two immortalized oral keratinocyte cell lines (NOK-SI, HOK16E6E7) were used in this study. HSC-3 was cultured in Dulbecco's modied Eagle's medium (DMEM; Gibco) containing 10% fetal calf serum (Gibco). SCC-9 was maintained in DMEM/Nutrient F-12 HAM (DMEM-F12; Gibco) containing 10% FBS, 2 mM L-glutamine, 50 U·mL^{-1} PenStrep, and 0.348% $NaHCO_3$. NOK-SI and HOK16E6E7 were cultured in keratinocyte growth medium (KGM) containing 0.15 mM calcium and EGF (Gibco). All cells were kept at 37 °C in a humidified incubator containing 5% CO_2.

Female BALB/c mice (5−6 weeks of age, 17−20 g) and female BALB/c athymic nude mice (4−5 weeks of age, 16−20 g) were purchased from the Animal Center of Sichuan University (Chengdu, China). All procedures followed the guidelines outlined in the "Principles of Laboratory Animal Care" (NIH) and were approved by the local Animal Care and Use Committee. Mice were housed five per cage in a temperature-controlled room (22 ± 1 °C) with a 12 h light/dark cycle. All mice had free access to deionized water and sterilized food and were quarantined this circumstance for at least 1 weeks before the experiments.

Preparation of SNNP. The J-TA L-ribonucleoside molecule (**1**) was designed and synthesized by our group. Then, certain amount of J-TA L-ribonucleoside was dissolved in distilled water (dH_2O); the solution was heated to ∼100 °C and allowed to cool to room temperature for ∼24 h.

Characterization of 5-FU-SNNP. The J-TA L-ribonucleosides were first dissolved in PBS; the solution was heated to ∼100 °C and allowed to cool to room temperature for ∼24 h. Then, the 5-FU was added in this solution and aged for 24 h to allow the drug-loading process to complete, which was verified by SEM and DLS. The drug loading and entrapment efficiency were determined as follows: 1 mL of drug loaded SNNP was introduced into EP tube and centrifuged at 13 000 rpm for 10 min. The concentration of 5-FU in collected the supernatants was determined by an ultraviolet spectrophotometer at 265 nm (DU-800 spectrophotometer, Beckman). All experiments were repeated three times. Drug loading (DL) and encapsulation efficiency (EE) of drug loaded SNNP were calculated according to eqs 1 and 2. The enzymatic degradation stability of SNNP was tested by incubating the samples of SNNP in preheated 90% fetal bovine serum (FBS) (1:9 v/v) for different times (1, 5, 12, and 24 h) at 37 °C using a thermal-shaker at 300 rpm *in vitro*. Then, SEM was employed to analyze the enzymatic degradation stability of SNNP through morphological change.

$$\mathrm{DL}\ (\%) = \frac{\text{Amount of drug}}{\text{SNNP} + \text{Theoretical drug}} \times 100 \qquad (1)$$

$$\mathrm{EE}\ (\%) = \frac{\text{Amount of drug}}{\text{Theoretical drug}} \times 100 \qquad (2)$$

***In Vitro* Drug Release Behavior.** To investigate the release behavior of 5-FU from the SNNP *in vitro*, a membraneless model was used. First, 200 μL of drug-loaded SNNP (the Drug Loading (DL) of SNNP was 35% and the Entrapment Efficiency (EE) of SNNP was 53%.) was immersed in 2 mL of PBS (pH = 7.4) and shaken at 100 rpm at 37 °C. Then, all the release media were collected and replaced with fresh release media at a specific time. After centrifugation at 13 000 rpm for 10 min, the supernatants of the removed release media were collected and stored at −20 °C for analysis. Finally, the concentration of 5-FU in collected supernatants was determined by an ultraviolet spectrophotometer at 265 nm (DU-800 spectrophotometer, Beckman). All release experiments were repeated three times.

Cell Viability Assay. The cytotoxicity of free SNNP was evaluated in both normal and cancer cell lines by viability of cells measured using 3-(4,5-dimethylthiozol-2-yl)-2,5-diphenyltetrazolium (MTT) (Sigma) assay as described previously.[56−58] Briefly, cells were cultured with SNNP at different concentrations of 100, 200, 300, 400, and 500 μg·mL^{-1} for 24, 48, and 72 h, respectively, using free medium as controls. Then, MTT solution (5 mg·mL^{-1} in PBS) was added to cell culture solution. Four hours later, the formazan crystals were dissolved in dimethyl sulfoxide (Sigma) and the absorbances were measured by Varioskan Flash (Thermo Scientific) at a wavelength of 570 nm. The relative cell viability (%) was presented by [OD] test wells/ [OD] control wells × 100%.

Hemolytic Test. Hemolytic test was performed as described.[49−52] Briefly, 2.5 mL of SNNP solution at different concentrations (100, 200, 300, 400, 500 μg·mL^{-1}) was added into 2.5 mL of 5% (v/v) RBC suspension and incubated for 3 h at 37 °C in a shaking water bath. Normal saline and distilled water were served as negative and positive controls, respectively. After incubation, all mixtures were centrifuged at 1500 rpm for 10 min, and the red color of the supernatant solution was regarded as hemolytic positive. Conversely, absolute achromatic of the supernatant indicated less likely to induce hemolytic.

Hemagglutination Assay. Hemagglutination test was performed as described previously.[49−52] In brief, 250 μL of blank SNNP solutions of different concentrations (100, 200, 300, 400, 500 μg·mL^{-1}) was mixed with 250 μL of rabbit erythrocyte suspension (2%) in V-shaped 24-well microtiter plates and incubated for 2 h at room temperature (RT) allowing hemagglutination to occur. A 2% erythrocyte suspension mixed with normal saline was used as negative control. Results were recorded by microscope at a magnification of 200×.

Acute Toxicity Test. In this study, complete blood count (CBC), serum biochemical analysis and histopathological study were used to evaluate the acute toxicity of SNNP *in vivo*. Forty female BALB/c mice were divided randomly into 5 groups. SNNP at different concentrations (0.5 , 2.5, and 5 mg·kg^{-1}) was injected intraperitoneally once a week using normal saline treated and nontreated mice as controls for 2 weeks. The body weight of mice was recorded every 3 days. After 15-days observation, all animals were killed and 1000 μL of blood sample was collected and divided into 2 parts: 200 μL with lihium heparin and 800 μL without lihium heparin. Serum was obtained by centrifugation at 2500 rpm for 15 min twice. Complete blood count (CBC) and serum biochemical indicators were measured by auto hematology analyzer (Cell-Dyn 3700, Abbott) and auto biochemistry analyzer (Roche cobas integra 400 plus, Roche, Switzerland), respectively. Organs including heart, liver, spleen, lung and kidney were drawn out, fixed immediately in 10% formaldehyde solution and embedded in paraffin and serially cut for histopathological examination by the hematoxylin and eosin (H&E) staining.

In this study, complete blood count analysis included markers such as white blood cells (WBC), red blood cells (RBC), platelet count (PLT), hemoglobin (HGB) and mean corpuscular volume (MCV). Liver function was evaluated by alanine aminotransferase (ALT), aspartate aminotransferase (AST), alkaline phosphatase (ALP), lactate dehydrogenase (LDH), total protein (TP) and albumin (ALB). Renal function was evaluated through uric acid (UA), blood urea nitrogen (BUN) and creatinine (CREA). Biochemical indicators for Blood lipids included triglyceride (TG), total cholesterol (CHOL), high density lipoprotein (HDL-C) and low density lipoprotein (LDL-C).

Serum Pharmacokinetics and Biodistribution Studies. Female BALB/c athymic nude mice were used to build OSCC xenograft mouse model. All animal care and *in vivo* experimental procedures were performed following NIH Principles of Laboratory Animal Care. A total of 2 × 10^6 HSC-3 cells were suspended in 100 μL of serum-free DMEM medium and injected subcutaneously into the right flank of mice to establish OSCC xenograft models.

On day 15, mice were randomized into 2 groups and received treatments *via* intravenous (iv) administration. Mice of control group were treated with 150 mg·kg^{-1} 5-FU and mice of test group were treated with 5 mg·kg^{-1} SNNP loading 150 mg·kg^{-1} 5-FU. Mice were sacrificed at various time points with blood and major organs collected for LC−MS/MS. Standards were prepared and measured along with the samples to calculate the percentage of the injected dose per gram of tissues (%ID/g). Statistics were based on standard deviations of 6 mice per group.

***In Vivo* Antitumor Efficacy Assay.** OSCC xenograft mouse model was built as described above. On day 5, the xenografts were detectable and mice were randomized into different groups and received treatments *via* intratumoral administration or intraperitoneal administration. Tumor growth and mouse body weight were monitored. The tumor size was measured twice a week using calipers. Tumor volume was calculated by the following formula: TV = $\pi/6 \times$ length $\times$ (width)^2. When the tumor sizes reached the maximum according to the guideline of Institutional Animal Care and Use Committee (IACUC), all mice were sacrificed by cervical dislocation.

Immunohistochemistry Assay. The xenografts were collected and fixed with paraformaldehyde for 48 h and processed for immunohistochemistry assessment of Ki67 (monoclonal antibody Ki67, Dako 1/200; abcam, Britain) as described before.[58] Proliferating cell was determined by positive immunostaining of Ki67. To calculate the proliferating rate of each tumor, 5 random areas within a section were selected and the total cell numbers and Ki67 positive cell numbers were counted at 200$\times$ magnification. The arithmetical mean proportion of positive Ki67 cells of the 5 areas represented the proliferating rate of the tumor. All micrographs were taken with Aperio Digital Pathology Systems.

TUNEL Assay. To detect apoptotic cells, the TUNEL assay was performed with the DeadEnd Fluorometric TUNEL System (Promega) according to the instructions from the manufacturer. Cells showing localized green fluorescence were regarded as apoptotic cells. The calculations of cell apoptosis rate of each tumor and the micrograph taken were conducted using the same methods as described in the immunohistochemistry assay section.

Statistical Analysis. Exiperiments were conducted in triplicates, or otherwise indicated. The data were presented as mean value $\pm$ SD (standard deviation). Statistical comparisons between different groups were evaluated by descriptive statistics, single-factor analysis of variance (ANOVA), and repeated measures analysis of variance assuming significant at P-value <0.05.

Conflict of Interest: The authors declare no competing financial interest.

Acknowledgment. The authors gratefully acknowledge support from the National Natural Science Foundation of China (81321002, 81270040, 81372890), the New Century Talents Support Program of MOE (NCET-12-0378), and the Open Foundation (SKLOD2015OF06, SKLOD201519) from the State Key Laboratory of Oral Diseases Sichuan University. We also thank the Core Facility of West China Hospital for the technical assisting and the Analysis and Testing Center of Sichuan University for helping us to process variable temperature NMR.

Supporting Information Available: The Supporting Information is available free of charge on the ACS Publications website at DOI: 10.1021/acsnano.5b04520.

Synthesis details, CD, TEM, VT-NMR, VT-FL, the drug loading efficiency and releasing behavior *in vitro* (Figures S1−S10, Table S1) (PDF)

REFERENCES AND NOTES

1. Mulvey, J. J.; Villa, C. H.; McDevitt, M. R.; Escorcia, F. E.; Casey, E.; Scheinberg, D. A. Self-Assembly of Carbon Nanotubes and Antibodies on Tumours for Targeted Amplified Delivery. *Nat. Nanotechnol.* **2013**, *8*, 763–771.
2. Devadasu, V. R.; Bhardwaj, V.; Ravi Kumar, M. N. V. Can Controversial Nanotechnology Promise Drug Delivery? *Chem. Rev.* **2013**, *113*, 1686–1735.
3. Irvine, D. J. One Nanoparticle, One Kill. *Nat. Mater.* **2011**, *10*, 342–343.
4. Tang, K.; Zhang, Y.; Zhang, H.; Xu, P.; Liu, J.; Ma, J.; Lv, M.; Li, D.; Katirai, F.; Shen, G.; et al. Delivery of Chemotherapeutic Drugs in Tumour Cell-derived Microparticles. *Nat. Commun.* **2012**, *3*, 1282.
5. Xiong, M.; Bao, Y.; Du, X.; Tan, Z.; Jiang, Q.; Wang, H.; Zhu, Y.; Wang, J. Differential Anticancer Drug Delivery with a Nanogel Sensitive to Bacteria-Accumulated Tumor Artificial Environment. *ACS Nano* **2013**, *7*, 10636–10645.
6. Weaver, C. L.; LaRosa, J. M.; Luo, X.; Tracy, X. Electrically Controlled Drug Delivery from Graphene Oxide Nanocomposite Films. *ACS Nano* **2014**, *8*, 1834–1843.
7. Tiwari, G.; Tiwari, R.; Sriwastawa, B.; Bhati, L.; Pandey, P.; Bannerjee, S. K. Drug Delivery Systems: An Updated Review. *Int. J. Pharm. Investig.* **2012**, *2*, 2–11.
8. Wei, T.; Liu, J.; Ma, H.; Cheng, Q.; Huang, Y.; Zhao, J.; Huo, S.; Xue, X.; Liang, Z.; Liang, X. Functionalized Nanoscale Micelles Improve Drug Delivery for Cancer Therapy *in Vitro* and *in Vivo*. *Nano Lett.* **2013**, *13*, 2528–2534.
9. Mackowiak, S. A.; Schmidt, A.; Weiss, V.; Argyo, C.; Schirnding, C.; Bein, T.; Bräuchle, C. Targeted Drug Delivery in Cancer Cells with Red-Light Photoactivated Mesoporous Silica Nanoparticles. *Nano Lett.* **2013**, *13*, 2576–2583.
10. Liu, Z.; Xiong, M.; Gong, J.; Zhang, Y.; Bai, N.; Luo, Y.; Li, L.; Wei, Y.; Liu, Y.; Tan, X. Legumain Protease-Activated TAT-Liposome Cargo for Targeting Tumors and Their Microenvironment. *Nat. Commun.* **2014**, 10.1038/ncomms5280.
11. Ha, C.; Gardella, J. A. Surface Chemistry of Biodegradable Polymers for Drug Delivery Systems. *Chem. Rev.* **2005**, *105*, 4205–4232.
12. Petros, R. A.; DeSimone, J. M. Strategies in The Design of Nanoparticles for Therapeutic Applications. *Nat. Rev. Drug Discovery* **2010**, *9*, 615–627.
13. Xu, C.; Xie, J.; Ho, D. Au-Fe_3O_4 Dumbbell Nanoparticles as Dualfunctional Probes. *Angew. Chem., Int. Ed.* **2008**, *47*, 173–176.
14. Liu, H. W.; Chen, C. H.; Tsai, C. L.; Lin, I. H.; Hsiue, G. H. Heterobifunctional Poly(ethylene glycol)-tethered Bone Morphogenetic Protein - 2 - stimulated Bone Marrow Mesenchymal Stromal Cell Differentiation and Osteogenesis. *Tissue Eng.* **2007**, *13*, 1113–1124.
15. Song, S.; Chen, Y.; Yan, Z.; Fenniri, H.; Webster, T. J. Self-Assembled Rosette Nanotubes for Incorporating Hydrophobic Drugs in Physiological Environments. *Int. J. Nanomed.* **2011**, *6*, 1035–1044.
16. Lee, H.; Lytton-Jean, A. K.; Chen, Y.; Love, K. T.; Park, A. I.; Karagiannis, E. D.; Sehgal, A.; Querbes, W.; Zurenko, C. S.; Jayaraman, M. Molecularly Self-Assembled Nucleic Acid Nanoparticles for Targeted *in Vivo* siRNA Selivery. *Nat. Nanotechnol.* **2012**, *7*, 389–393.
17. Walsh, A. S.; Yin, H.; Erben, C. M.; Wood, M. J. A.; Tuberfield, A. J. DNA Cage Delivery to Mammalian Cells. *ACS Nano* **2011**, *5*, 5427–5432.
18. Allain, V.; Bourgaux, C.; Couvreur, P. Self-Assembled Nucleolipids: From Supramolecular Structure to Soft Nucleic Acid and Drug Delivery Devices. *Nucleic Acids Res.* **2012**, *40*, 1891–1903.
19. Khiati, S.; Luvino, D.; Oumzil, K.; Chauffert, B.; Camplo, M.; Barthelemy, P. NucleosideLipid-Based Nanoparticles for Cisplatin Delivery. *ACS Nano* **2011**, *5*, 8649–8655.
20. Maksimenko, A.; Mougin, J.; Mura, S.; Sliwinski, E.; Lepeltier, E.; Bourgaux, C.; Lepêtre, S.; Zouhiri, F.; Desmaële, D. Couvreur, Patrick. Polyisoprenoyl Gemcitabine Conjugates Self-Assemble as Nanoparticles, Useful for Cancer Therapy. *Cancer Lett.* **2013**, *334*, 346–353.
21. Daman, Z.; Ostad, S.; Amini, M.; Gilani, K. Preparation, Optimization and *in Vitro* Characterization of Stearoyl-Gemcitabine Polymeric Micelles: A Comparison with Its Self-Assembled Nanoparticles. *Int. J. Pharm.* **2014**, *468*, 142–151.
22. Zhao, H.; Huang, W.; Wu, X.; Xing, Z.; He, Y.; Chen, Q. Different Superstructures Formed by Janus-Type Nucleosides. *Chem. Commun.* **2012**, *48*, 6097–6098.

23. Zhao, H.; He, S.; Yang, M.; Guo, X.; Xin, G.; Zhang, C.; Ye, L.; Chu, L.; Xing, Z.; Huang, W. Micro-flowers Changing to Nano-Bundle Aggregates by Translocation of The Sugar Moiety in Janus TA Nucleosides. *Chem. Commun.* **2013**, *49*, 3742–3744.
24. Zhao, H.; Guo, X.; He, S.; Zeng, X.; Zhou, X.; Zhang, C.; Hu, J.; Wu, X.; Xing, Z.; Chu, L.; et al. Complex Self-Assembly of Pyrimido[4,5-d]pyrimidine Nucleoside Supramolecular Structures. *Nat. Commun.* **2014**, 10.1038/ncomms4108.
25. Sasahira, T.; Ueda, N.; Yamamoto, K.; Kurihara, M.; Matsushima, S.; Bhawal, U. K.; Kirita, Tadaaki; Kuniyasu, H. Prox1 and FOXC2 Act as Regulators of Lymphangiogenesis and Angiogenesis in Oral Squamous Cell Carcinoma. *PLoS One* **2014**, *9*, e92534.
26. Salahshourifar, L.; Vincent-Chong, V. K.; Kallarallal, T. G.; Zain, R. B. Genomic DNA Copy Number Alterations from Precursor or Allusions to Oral Squamous Cell Carcinoma. *Oral Oncol.* **2014**, *50*, 404–412.
27. Khandelwal, S.; Solomon, M. C. Cytomorphological Analysis of Keratinocytes in Oral Smears from Tobacco Users and Oral Squamous Cell Carcinoma Lesions — A Histochemical Approach. *Int. J. Oral Sci.* **2010**, *2*, 45–52.
28. Jiménez, I. R.; Martín, M. N. C.; Luna, A.; Delgado, L. C. Functional Imaging in Oncology. In *Head and Neck Cancer*; Luna, A., Vilanova, J. C., Hygino Da Cruz, L. C., Jr., Rossi, S. E., Eds.; Springer-Verlag: Berlin, 2014; pp 703−720.
29. Chen, X. R.; Lu, R.; Dan, H. X.; Liao, G.; Zhou, M.; Li, X. Y.; Ji, N. Honokiol: A Promising Small Molecular Weight Natural Agent for The Growth Inhibition of Oral Squamous Cell Carcinoma Cells. *Int. J. Oral Sci.* **2011**, *3*, 34–42.
30. Marsh, D.; Suchak, K.; Moutasim, K. A.; Valllath, S.; Hopper, C.; Jerjes, W.; Upile, T.; Kalavrezos, N.; Violette, S. M.; Weinreb, P. H.; et al. Stromal Features Are Predictive of Disease Mortality in Oral Cancer Patients. *J. Pathol.* **2011**, *223*, 470–481.
31. Mydlarz, W. K.; Hennessey, P. T.; Califano, J. A. Adavanced and Perspectives in The Molecular Diagnosis of Head and Neck Cancer. *Expert Opin. Med. Diagn.* **2010**, *4*, 53–65.
32. Heidelberger, C.; Chaudhuri, N. K.; Danenberg, P.; Mooren, D.; Griesbach, L.; Duschinsky, R.; Schnitzer, R. J.; Pleven, E.; Scheiner, J. Fluorinated Pyrimidines, A New Class of Tumor Inhibitory Compounds. *Nature (London, U. K.)* **1957**, *179*, 663–666.
33. Diasio, R. B.; Lu, Z. Dihydropyrimidine Dehydrogenase Activity and Fluorouracil Chemotherapy. *J. Clin Oncol.* **1994**, *12*, 2239–2242.
34. Schilsky, R. L.; Hohneker, J.; Ratain, M. J.; Janisch, L.; Smetzer, L.; Lucas, V. S.; Khor, S. P.; Diasio, R.; Von Hoff, D. D.; Burris, H. A. Phase I Clinical and Pharmacologic Study of Eniluracil Plus Fluorouracil in Patients with Advanced Cancer. *J. Clin. Oncol.* **1998**, *16*, 1450–1457.
35. Gamelin, E. C.; Danquechin-Dorval, E. M.; Dumesnil, Y. F.; Maillart, P. J.; Goudier, M. J.; Burtin, P. C.; Delva, R. G.; Lortholary, A. H.; Gesta, P. H.; Larra, F. G. Relationship between 5-Fluorouracil (5-FU) Dose Intensity and Therapeutic Response in Patients with Advanced Colorectal Cancer Receiving Infusional Therapy Containing 5-FU. *Cancer* **1996**, *77*, 441–451.
36. Aranda, E.; Diaz-Rubio, E.; Cervantes, A.; Anton-Torres, A.; Carrato, A.; Massuti, T.; Tabernero, J. M.; Sastre, J.; Tres, A.; Aparicio, J.; et al. Randomized Trial Comparing Monthly Low-Dose Leucovorin and Fluorouracil Bolus with Weekly High-Dose 48-h Continuous-Infusion Fluorouracil for Advanced Colorectal Cancer: a Spanish Cooperative Group for Gastrointestinal Tumor Therapy (TTD) Study. *Ann. Oncol.* **1998**, *9*, 727–731.
37. Shirasaka, T.; Yamamitsu, S.; Tsuji, A.; Terashima, M.; Hirata, K. Conceptual Changes in Cancer Chemotherapy-Biochemical Modulation of 5-FU. *Gan To Kagaku Ryoho* **2000**, *27*, 832–845.
38. Tummala, S.; Kumar, M. N. S; Prakash, A. Formulation and Characterization of 5-Fluorouracil Enteric Coated Nanoparticles for Sustained andLocalized Release in Treating Colorectal Cancer. *Saudi Pharm. J.* **2015**, *23*, 308–314.
39. Chen, L.; She, X.; Wang, X.; He, L.; Shigdar, S.; Duan, W.; Kong, L. Overcoming Acquired Drug Resistance in Colorectal Cancer Cells by Targeted Delivery of 5-FU with EGF Grafted Hollow Mesoporous Silica Nanoparticles. *Nanoscale* **2015**, *7*, 14080–14092.
40. Timothy, C. J.; Nora, K.; Eric, M. P.; Omid, C. F.; Robert, L.; Stephen, J. L. Nanoparticle Encapsulation of Mitaplatin and Effect Thereof on *in Vivo* Properties. *ACS Nano* **2013**, *7*, 5675–5683.
41. Kleandrova, V. V.; Luan, F.; González-Díaz, H.; Ruso, J. M.; Melo, A.; Speck-Planche, A.; Cordeiro, M. N. Computational Ecotoxicology: Simultaneous Prediction of Ecotoxic Effects of Nanoparticles under Different Experimental Conditions. *Environ. Int.* **2014**, *73*, 288–294.
42. Rosenberger, I.; Schmithals, C.; Vandooren, J.; Bianchessi, S.; Milani, P.; Locatelli, E.; Israel, L. L.; Hübner, F.; Matteoli, M.; Lellouche, J. P.; et al. Physico-Chemical and Toxicological Characterisation of Iron-Containing Albumin Nanoparticles as Platforms for Medical Imaging. *J. Controlled Release* **2014**, *194*, 130–137.
43. Chauhan, D.; Singh, A. V.; Aujay, M.; Kirk, C. J.; Bandi, M.; Ciccarelli, B.; Raje, N.; Richardson, P.; Anderson, K. C. A Novel Orally Active Proteasome Inhibitor ONX 0912 Triggers *in Vitro* and *in Vivo* Cytotoxicity in Multiple Myeloma. *Blood* **2010**, *116*, 4906–4915.
44. Horcajada, P.; Chalati, T.; Serre, C.; Gillet, B.; Sebrie, C.; Baati, T.; Eubank, J. F.; Daniela, H.; Clayette, P.; Kreuz, C.; et al. Porous Metal−Organic-Framework Nanoscale Carriers as a Potential Platform for Drug Delivery and Imaging. *Nat. Mater.* **2010**, *9*, 172–178.
45. Pelaz, B.; Jaber, S.; Jimenez de Aberasturi, D.; Wulf, V.; Feldmann, J.; Gaub, H. E.; Josephson, L.; Kagan, C. R. The State of Nanoparticle-Based Nanoscience and Biotechnology: Progress, Promises, and Challenges. *ACS Nano* **2012**, *6*, 8468–8483.
46. AshaRani, P. V.; Mun, G. L. K.; Hande, M. P.; Valiyaveettil, S. Cytotoxicity and Genotoxicity of Silver Nanoparticles in Human Cells. *ACS Nano* **2009**, *3*, 279–290.
47. Dobrovolskaia, M. A.; Clogston, J. D.; Neun, B. W.; Hall, J. B.; Patri, A. K.; McNeil, S. E. Method for Analysis of Nanoparticle Hemolytic Properties *in Vitro*. *Nano Lett.* **2008**, *8*, 2180–2187.
48. Gou, M.; Men, K.; Zhang, J.; Li, Y.; Song, J.; Luo, S.; Shi, H.; Wen, Y.; Guo, G.; Huang, M. Efficient Iinhibition of C-26 Colon Carcinoma by VSVMP Gene Delivered by Biodegradable Cationic Nanogel Derived from Polyethyleneimine. *ACS Nano* **2010**, *4*, 5573–5584.
49. Gupta, N. K.; Tomar, P.; Sharma, V.; Dixit, V. K. Development and Characterization of Chitosan Coated Poly-(Varepsilon-Caprolactone) Nanoparticulate System for Effective Immunization Against Influenza. *Vaccine* **2011**, *29*, 9026–9037.
50. Fischer, D.; Li, Y.; Ahlemeyer, B.; Krieglstein, J.; Kissel, T. *In vitro* Cytotoxicity Testing of Polycations: Influence of Polymer Structure on Cell Viability and Hemolysis. *Biomaterials* **2003**, *24*, 1121–1131.
51. Kunwar, A.; Bansal, P.; Kumar, S. J.; Bag, P. P.; Paul, P.; Reddy, N. D.; Kumbhare, L. B.; Jain, V. K.; Chaubey, R. C.; Unnikrishnan, M. K.; et al. *In vivo* Radioprotection Studies of 3,3 '-Diselenodipropionic Acid, a Selenocystine Derivative. *Free Radical Biol. Med.* **2010**, *48*, 399–410.
52. Xiong, L. Q.; Yang, T. S.; Yang, Y.; Xu, C. J.; Li, F. Y. Long-Term *in Vivo* Biodistribution Imaging and Toxicity of Polyacrylic Acid-Coated Upconversion Nanophosphors. *Biomaterials* **2010**, *31*, 7078–7085.
53. Shen, J. L.; Xu, R.; Mai, J. H.; Kim, H. C.; Guo, X. J.; Qin, G. T.; Yang, Y.; Wolfram, J.; Mu, C. F.; Xia, X. J.; et al. High Capacity Nanoporous Silicon Carrier for Systemic Delivery of Gene Silencing Therapeutics. *ACS Nano* **2013**, *7*, 9867–9880.
54. Yin, W. Y.; Yan, L.; Yu, J.; Tian, G.; Zhou, L. J.; Zheng, X. P.; Zhang, X.; Yong, Y.; Gu, Z. J.; Zhao, Y. L. High- Throughput Synthesis of Single-Layer MoS2 Nanosheets as a Near-Infrared Photothermal-Triggered Drug Delivery for Effective Cancer Therapy. *ACS Nano* **2014**, *8*, 6922–6933.

55. Mahmoudi, M.; Hofmann, H.; Rothen-Rutishauser, B.; Petri-Fink, A. Assessing The *in Vitro* and *in Vivo* Toxicity of Superparamagnetic Iron Oxide Nanoparticles. *Chem. Rev.* **2012**, *112*, 2323–2338.
56. MacKay, J. A.; Chen, M. N.; McDaniel, J. R.; Liu, W. G.; Simnick, A. J.; Chilkoti, A. Self-Assembling Chimeric Polypeptide-Doxorubicin Conjugate Nanoparticles That Abolish Tumors after a Single Injection. *Nat. Mater.* **2009**, *8*, 993–999.
57. Li, S. D.; Chen, Y. C.; Hackett, M. J.; Huang, L. Tumor-Targeted Delivery of siRNA by Self-Assembled Nanoparticles. *Mol. Ther.* **2008**, *16*, 163–169.
58. Wang, X.; Wang, Y. X.; Lydia, K.; Ada, G.; Paraskevi, G.; Edwin, H. S.; Mourad, T.; Chen, Z.; Nie, S. A Folate Receptor-Targeting Nanoparticle Minimizes Drug Resistance in a Human Cancer Model. *ACS Nano* **2011**, *5*, 6184–6194.